JITH 2017
18èmes Journées Internationales de Thermique (JITH 2017)
Monastir (Tunisie), 25 - 27 Octobre 2017

Numerical modeling of mass and heat transfer phenomena in the anode porous micro-structure of a solid oxide fuel cell using Lattice Boltzmann Method (LBM)

Dhouha Ben Hamadou, Amal Elleuch and Kamel Halouani

[1]UR-Micro Electro Thermal Systems, National Engineering School of Sfax, University of Sfax
IPEIS, BP: 1172, 3018 Sfax, Tunisia
amal-elleuch@hotmail.com, **kamel_ipeis@yahoo.fr**

Abstract: Today's world needs highly efficient systems that can fulfill the growing demand for energy. Among the promising solutions are fuel cells. Solid Oxide Fuel cell (SOFC) is considered as an alternative eco-friendly and efficient solution for electrical and thermal power generation in the near future. Mathematical modeling of transport phenomena within a SOFC has been the subject of various investigations. Recent advances in the lattice Boltzmann method (LBM) have made possible the simulation of mass transfer in complex geometry i.e. the porous microstructure of SOFC anode. Lattice Boltzmann method (LBM) modeling of SOFC mass transfer phenomena can give accurate understanding and description of the pore-level design and can have a significant impact on the SOFC microstructure optimization and thereafter on the efficiency and durability enhancement of the cell. As an example application, a one species LBM mass diffusion model coupled with a Thermal Lattice Boltzmann Method (TLBM) is developed here. Both artificially and real scanned image porous media were treated as porous anode to provide geometry input to the LBM model. Some preliminary, two dimensional (2D) results are presented for velocity profiles, density and thermal distribution inside the SOFC anode. Future work involves extending the LBM to multi-component mass transfer model and validation of model predictions with experiments.

Keywords: Lattice Boltzmann Method, SOFC, anode, Modeling, heat and mass transfer.

1. Introduction

Solid oxide fuel cell (SOFC) is an energy conversion system that converts chemical energy of several fuels to electricity with high efficiency. Conventional SOFC essentially consists of porous anode and cathode layers separated by a dense ceramic electrolyte. These electrodes have pore sizes ranging from nanometers to micrometers. The anode is a ceramic-metal composite (cermet). The electrolyte has the ability to conduct oxide ions (O^{2-}) at high temperatures. Mass transfer of the H_2 fuel takes place from the gas channel and through the anode pore space to the electrochemical reaction sites called three-phase boundary (TPB) at the anode/electrolyte interface. Oxygen ions travel through the electrolyte and through part of the anode structure until reaching the anode TPB. Electrochemical reactions at the anode TPB essentially lead to the combination of the oxygen ions with fuel (H_2) to produce (H_2O) and free electrons (2e-). The H_2O must then diffuse back through the pores in the anode to the gas channel while the electrons must travel through the electrically conducting solid phase of the anode to the current collector to provide useful work.
Because the SOFC operates at a high temperature, hydrocarbons fuels can be directly reformed within the anode to generate H_2, eliminating the need for pure H_2 as fuel. This reforming takes place via heterogeneous and gas shift reactions at active sites [1]. Significant technological and economic hurdles must be overcome before finding widespread acceptance for SOFCs. Some of the challenges include durable designs that can withstand higher temperatures (up to 750 °C) and ensure an enhancement in the delivered power density of the SOFC via microstructure optimization.
Mathematical modeling can play a crucial role in predicting SOFC performance under a wide range of operating conditions via a deeper understanding of the underlying transport phenomena that drive its operation.

Because of the intimate coupling between mass transport, heat transport and electrochemical reactions inside the SOFC and because of the complex porous geometry, modeling transport processes in a SOFC is not an easy task even if detailed geometric information about the pore structure is available.

The majorities of SOFC models are developed at the macro scale and approximate the electrode microstructure by parameters like pore diameter, porosity and tortuosity and adopt a system level approach to predict the SOFC performance. While this is useful, it does not permit a deeper understanding of the influence of electrode geometry at the micro scale. The electrode microstructure is quite complex and, until recently, the use of reconstructed 3D images as inputs for SOFC transport models is scarce [2]. At micro- and meso-scale, Lattice Boltzmann Method (LBM) appeared as powerful tools for modeling several engineering applications including especially complex geometries. Although LBM is a relatively new actor among the numerical modeling methods, some works has already been carried out on solid oxide fuel cells. LBM has recently compared with conventional methods such as FDM, FEM and FVM when modeling SOFCs transport processes [3].

The LBM method is described in detail by Joshi research group [4-7] and is used usually to describe the mass diffusion process from 2D to 3D system. In their recent work, The LBM was used to study the 3D mass diffusion of three species (H_2, H_2O, and N_2) in the pore phase of a porous SOFC anode. The method used is an extension of a 2D LBM model [7] to study mass transport in SOFC anodes [6]. They modeled 3D porous anode geometry using a set of randomly packed and overlapping solid spheres. Results using this simple geometry model are compared with results for an actual SOFC anode geometry obtained using X-ray computed tomography. Using the LBM micro-model, the effective diffusivity which is a parameter widely used in models through several empirically relationships is calculated for different geometries and for a range of porosity values, both for the 3D sphere packing model and for the real geometry. They used the LBM model then to predict species mole fractions. They subsequently used the mole fraction variation to calculate the concentration losses and compared predictions with their previous 2D model results. They demonstrated the model capability in accurately predicting SOFC concentration polarization losses.

The LBM model is a powerful tool that can be used to simulate SOFC electrodes behavior without empirically modifying the diffusion coefficients using medium porosity and tortuosity when detailed imaged geometry data are used as input for the LBM model. Grew et al. [8] examined the role and importance of the porosity and tortuosity of the electrode structure, catalytically active area and species mole fractions at the fuel channel on the direct methane internal reforming using a coupled electrochemical kinetic based on detailed reforming reaction mechanism with a 5 species mass transfer LBM model. Among their more interesting results, the inlet CH_4 and H_2 mole fractions have been systematically varied demonstrating a strong coupling between the structure, transport and reaction processes.

An LBM model using 3D micro-structural data and active-TPB density was applied by Guan et al. [9] to simulate the ternary gas diffusion (H_2, H_2O and N_2) in the connected pore channel of a SOFC. The effect of 3D microstructure and active-TPB density on the gas transport is discussed, and the concentration polarizations of the anodes during thermal cycling were calculated. Obtained results by the above-mentioned non-destructive imaging technology indicate that the pore connectivity and active-TPB density influence the concentration polarizations at the TPB sites.

Although the simulation of isothermal problems has reached a great success, the development of a thermal model is always a challenge. All the developed thermal models can be classified into two main approaches which are: The multispeed approach and the double distribution function approach. The multispeed approach, introduced by Garcia et al. [10], used a single distribution function f, similarly to the previous approach (mass problem), and a higher order of velocities to take into account the temperature field. It has been shown that this model suffers from stability problems and can be applied only for a limited temperature range [10]. Recently, Abbassi et al. [11] developed a thermal LBM method to study the radiative effect on the temperature distribution through a planar SOFC system. They used a single distribution function to get the temperature profile. The reaction – diffusion processes are not investigated. The 2D thermal model results showed that the highest temperature is located in the electrolyte layer. They demonstrated that heat transfer via radiation could be neglected despite the use of SOFC solid ceramics layers and higher operating temperature. They demonstrated later that the radiative effect does not change the temperature profile while it causes a slight decrease in the temperatures inside the SOFC domains [12]. Shan [13] improved McNamara model by simulating the temperature field using an additional component (an additional distribution function$g$), as a way to avoid the numerical instability. This was the first attempt to utilize double distribution function models. Stability of thermal models was improved further, in 2003, by Lallemand and Luo [14]. Several models have been performed based on the latter model approach beginning with the work of He et al. [15] who introduced an energy distribution function. It consists on an improvement to the quasi-double distribution function model of Shan, since it takes into account the viscous dissipation effect and compression work.

Peng et al. [16] worked on the same problem as He et al., but neglected compression work and viscous dissipation for incompressible limit, a fact that simplifies considerably the model initially proposed. Based on Peng work, D'Orazio and Succi [17] added a force term to take into account the viscous heating. Advances have

been made for thermal double distribution function models until developing a simplified thermal model by Shi et al. [18] in 2004. Azwadi and tanahachi [19] have utilized the same model of Shi et al. [18] but used two different lattice models for each distribution function: D2Q9 for solving mass or momentum problem using the distribution function f, and D2Q4 for solving temperature field using the distribution function g.

In the present paper, Shi et al. [18] thermal LBM model will be adopted for simulating temperature profile in the porous anode layer of a solid oxide fuel cell. Globally, various aspects have been studied, from treating mass transfer problem to electrochemical reactions inside the SOFCs. Nevertheless, thermal aspect taking into account the energy field in the simulation, i.e. coupling heat and mass transfer investigation inside the solid oxide fuel cell is quite rare and is the main subject of this paper. Then, a non-isothermal flows will be simulated as an application of the thermal Lattice Boltzmann method, coupling thermal and mass phenomena. A first benchmark of a flow in a rectangular channel will be discussed. Hence, simulation of velocity and thermal flow around a hot sphere will be performed. A further step towards modeling mass and thermal flow in the porous SOFC anode is the simulation of flows in two anode geometries. One is build up with an artificial porous media where randomly placed spheres are heated and the other one is obtained by image treatment carried to a real scanning electron microscopy (SEM) image.

2. Lattice Boltzmann Method

2.1. LBM modeling basics and mathematical formulation

In the last few years, Lattice Boltzmann Method (LBM) was shown as a promising alternative to the traditional CFD approach that is well-suited to simulate fluid flow and diffusion through porous media involving single or multiple liquid or gas components. LBM is not the first method in the discrete approach. It is closely related to the family of methods, which ultimately preceded it, the Lattice Gas Automata (LGA).
The term "lattice gas" refers to a family of cellular automata [20-21], which have been proposed as a new technique for the numerical study of Navier Stokes equations, and are based on simple microscopic systems substituting the direct integration of partial differential equations.

LBM is known as a bridge between the continuum methods and the discrete methods thanks to its ability to study the behavior of a package of particles instead of a single sub-atomic particle. It permits to make approximations of several physical phenomena at the micro and also macro-scale level through knowledge of the average characteristics of the package of particles. Conventional CFD methods use fluid density, velocity and pressure as the primary variables, while LBM uses a more fundamental approach with the so-called particle velocity distribution function (PDF). The PDF permits the analysis of the millions of particles motion according to a statistical description. PDF is a function of the position and time of the package of particles which is defined as the number of particles of the same species traveling a particular direction with a particular velocity.
The domain that will be solved has to be divided into lattice points called also lattice nodes. Each lattice point has velocity connections with its neighborhood. The common way to represent the lattice arrangement is called DnQm where n is the space dimension and m refers to the number of discrete velocities used in the lattice. For 2D flows, the Boltzmann model with nine velocities denoted by D2Q9 is the most used scheme (Figure 1). To simulate 3D flows, there are different lattice models such as D3Q15, D3Q19, D3Q27... etc. The choice of a Lattice depends on the required accuracy, the complexity of the problem, memory space available etc...

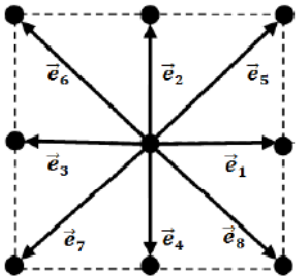

Figure 1: Illustration of a lattice node of the D2Q9 model

The LBM essentially consists of two basic steps that are carried out at each node point that is not inside an obstacle: streaming and collision. The collision process is local, while streaming process is the only way to propagate the information from one node to the neighboring nodes. Streaming represents movement of particles of each species along specified, nearest neighbor lattice directions $e_\alpha^i\{\alpha = 0,1,2,3,4,5,6,7,8\}$. These velocity directions are based on the D2Q9 model adopted in this work. The collision term represents interactions between the particles as they arrive at any given node.

The collision operator used in this work for the PDF is the Bhatnagar, Gross and Krook (BGK) collision operator which is the most used one in LBM models thanks to its simplicity, linearity, and so the low programming cost. It proved a good accuracy in various simulation cases especially in the case of single phase problems. It was used also in solving problems of chemically reacting gas mixtures, i.e multi-component flows [22]. BGK model has some shortcomings that came mainly from the single relaxation parameter of the collision term. In fact, with a single relaxation time constant, we cannot adjust independently the macroscopic transport coefficients, such as bulk and shear viscosities. In order to increase the number of tunable coefficients, we need more relaxation parameters, such as the case of the Multiple-Relaxation-Time (MRT) model [23].

The latter two steps are combined together in Eq. (1), which is called the Lattice Boltzmann equation:

$$f\left(x + v_{ix}\,\Delta t\,, y + v_{iy}\,\Delta t\,, t + \Delta t\right) - f(x,y,t) = \frac{-1}{\tau_f}\left(f_i(x,y,t) - f_{eq,i}(x,y,t)\right) \quad (1)$$

The relaxation time for the distribution function $f\left(\tau_f\right)$ is given in terms of kinematic viscosity:

$$\nu = \frac{1}{3}\left(\tau_f - \frac{1}{2}\right) \qquad (2)$$

The equilibrium distribution function is expanded using the second order Taylor expansion of e^x and given as follows for every direction i of the domain:

$$f_{eq,i} = \omega_i \rho \left[1 + \frac{3(v_i.u)}{c^2} + \frac{9}{2}\frac{(v_i.u)^2}{c^4} - \frac{3}{2}\frac{u^2}{c^2}\right] \quad (3)$$

Where ρ is the density, v is the particle velocity and u is the fluid velocity.The lattice speed ($c = \Delta x/\Delta t$) is fixed to 1 as discrete length step Δx and discrete time step Δt are often chosen as 1.
For the selected D2Q9, the weight factors (ω_i) are:

$$\omega_i = \begin{cases} 4/9 & i = 0 \\ 1/9 & i = 1,2,3,4 \\ 1/36 & i = 5,6,7,8 \end{cases} \quad (4)$$

The discrete velocity (v_i) in every direction i represents the coordinates of vectors in the Lattice model and are taken as follows for D2Q9 scheme.

$$v_i = \begin{cases} (0,0) & i = 0 \\ (1,0),(0,1),(-1,0),(0,-1) & i = 1,2,3,4 \\ (1,1),(-1,1),(-1,-1),(1,-1) & i = 5,6,7,8 \end{cases} \quad (5)$$

The speed of sound(c_s) for the D2Q9 is constant ($c_s^2 = 1/3$) and is function of the lattice velocity ($c_s = \frac{c}{\sqrt{3}} = \sqrt{K_B T/m}$. The equilibrium distribution function related to the speed of sound will be:

$$f_{eq,i} = \omega_i \rho \left[1 + \frac{(v_i.u)}{c_s^2} + \frac{(v_i.u)^2}{2\,c_s^4} - \frac{u^2}{2\,c_s^2}\right] \quad (6)$$

As elucidated in previous sections, Lattice Boltzmann Method solves the Boltzmann equation at a mesoscopic scale. Nevertheless, the purpose is to find the numerical results solved by the Navier-Stokes equations. That's why we need to recover the Navier-Stokes equations at the macroscopic scale. The procedure used to recover these equations is the Chapman-Enskog, a multi-scale analysis, introduced separately by Chapman and Enskog between 1910 and 1920 [24]. The expansion is elaborated using two main parameters which are the Mach number, and Knudsen number. The latter one is defined as the ratio between the mean free path of a gas molecule and a macroscopic length scale.

Once Eq. (1) is solved, the macroscopic variables (ρ, u) in the discrete form can be recovered by taking the weight $m = 1$:

$$\rho(x,y,t) = \sum_{i=0}^{8} f_i(x,y,t) \quad (7)$$

$$u(x,y,t) = \frac{1}{\rho}\sum_{i=0}^{8} v_i f_i(x,y,t) \quad (8)$$

Another distribution function used to simulate the temperature field is g and is expressed as follows:

$$g\left(x + v_{ix}\,\Delta t\,, y + v_{iy}\,\Delta t\,, t + \Delta t\right) - g(x,y,t) = \frac{-1}{\tau_T}\left(g_i(x,y,t) - g_{eq,i}(x,y,t)\right) \qquad (9)$$

Where τ_T represent the relaxation timefor the distribution function $g$and is given in terms of thermal diffusivity (Eq.10):

$$\alpha = \frac{1}{3}\left(\tau_T - \frac{1}{2}\right) \quad (10)$$

The equilibrium distribution $g_{eq,i}$ is given by:

$$g_{eq,i} = \omega_i \rho T\left[1 + \frac{(v_i.u)}{c_s^2}\right] \quad (11)$$

The macroscopic temperature is computed as follows:

$$\rho\, T(x,y,t) = \sum_{i=0}^{8} g_i(x,y,t) \quad (12)$$

The coupling between mass and heat transfer phenomena occurs in the exchange of velocity field between the two distribution functions (f and g). In fact, the computation of g_i in the collision step utilizes the values of ($g_{eq,i}$) which in its turn contains the velocity values (Eq.11). These velocity values also occur in the equilibrium function ($f_{eq,i}$). Therefore a coupling mass-temperature is proved.

The relation between the SI units and the Lattice units is formed by using the parameters Δx and Δt, which are the discrete space step and time step, respectively. First the conversion to dimensionless system was carried after choosing the appropriate characteristic parameters including the characteristic length ℓ_0, time t_0 and velocity u_0. The obtained dimensionless parameters (t_d, ℓ_d, u_d, ν_d and Re_d) are defined in Table 1.

Table 1: Dimensionless parameters.

Dimensionless time	$t_d = t_p/t_0$
Dimensionless length	$\ell_d = \ell_p/\ell_0$
Dimensionless velocity	$u_d = \frac{t_0}{\ell_0} u_p$
Dimensionless viscosity	$\nu_d = \frac{t_0}{\ell_0^{\,2}} \nu_p$
Dimensionless Reynolds	$Re_d = \frac{u_{0,d}\ell_{0,d}}{\nu_d}$

The discretization is handled through the equations given below defining the discrete space interval Δx as the reference length divided by the number of cells N usedto discretize this length. In the same way, Δt is defined as the reference time divided by the number of iteration steps (N_{iter}) needed to reach this time. Both reference variables are unity in the dimensionless system.

$$\Delta x = \frac{1}{N} \quad (13)$$

$$\Delta t = \frac{1}{N_{iter}} \quad (14)$$

Similarly to the renormalization from physical system to dimensionless system, the discrete parameters implemented in the LBM model are defined in Table 2.

Table 2: Lattice parameters equations.

Length in Lattice units	$\ell_{lb} = \ell_d/\Delta x$
Velocity in Lattice units	$u_{lb} = \frac{\Delta t}{\Delta x}$
Kinematic viscosity in Lattice units	$\nu_{lb} = \frac{\Delta t}{\Delta x^2} \nu_d$
Reynolds in Lattice units	$Re_{lb} = \frac{u_{0,lb}\ell_{0,lb}}{\nu_{lb}}$

Using the lattice units, the relationship between the relaxation time and the lattice viscosity is given by:

$$\tau = \frac{\nu_{lb}}{c_s^2} + \frac{1}{2} \quad (15)$$

2.2. Boundary conditions

The boundary conditions in the LBM do not have the same concept as the boundary conditions applied in computational fluid dynamics (CFD) models. In LBM, the role of boundary conditions is evaluating the unknown distribution functions f_i at every boundary. Figure 2 shows the unknown distribution functions that we need to calculate at every boundary. Note that the unknown functions are those pointing to the inside of the domain.

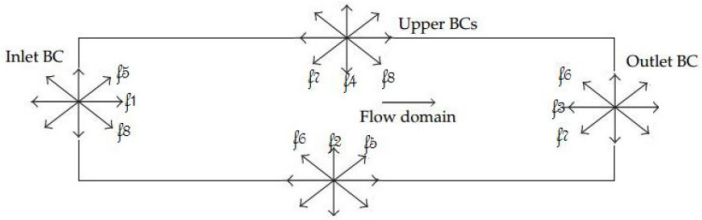

Figure 2: unknown distribution functions in each boundary.

2.2.1. Mass boundary conditions

Bounce-back boundaries, also called no-slip boundary conditions, are the typical boundaries for simulating the interaction of fluids with a non-moving wall without slip. In addition, they are used to simulate the flow around obstacles. They are largely used because they ensure the mass, momentum and energy conservation, apart from their simplicity, their good numerical stability and accuracy. As the name implies, when a particle is coming towards the solid boundary it bounces back into the flow domain. In this work, Full-way bounce-back is used to implement no-slip (zero-velocity) walls. f_4, f_7, f_8 are known from streaming process. It is assumed that when these known distribution functions hit the wall, bounce back to the solution domain. Therefore, $f_5 = f_7$, $f_2 = f_4$ and $f_6 = f_8$.

When the periodic boundaries are applied in one direction, the domain of the simulation changes to cylindrical geometry as shown in Figure 3. The nodes placed in the boundary, where the periodic condition is applied, have its neighboring nodes on the opposite boundary [25]:

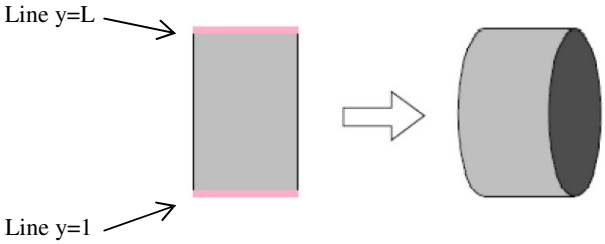

Figure 3: cylindrical shape of the domain after periodic boundary conditions applications.

The distribution function f_4, f_7, f_8 are unknown on the line $(y = L)$ and f_2, f_5, f_6 are unknown on the line $(y = 1)$. The periodic boundary is written as follows:

- Along line $(y = L)$: ${f_4}^{y=L} = {f_4}^{y=1}$, ${f_7}^{y=L} = {f_7}^{y=1}$, ${f_8}^{y=L} = {f_8}^{y=1}$
- Along line $(y = 1)$: ${f_2}^{y=1} = {f_2}^{y=L}$, ${f_5}^{y=1} = {f_5}^{y=L}$, ${f_6}^{y=1} = {f_6}^{y=L}$

Zou and He [26] introduced the velocity (Von-Neumann) boundary condition that implements a certain flux condition on the boundary [27]. A velocity is specified $u = (u_x, u_y)$ at the boundary, from which a density is computed, and thus, the distribution function values are calculated to achieve the distribution that implies the fixed velocity. In this work, the conditions of this type of boundary conditions applied at the west boundary are given by the following equations:

$$\rho = \frac{f_0 + f_2 + f_4 + 2(f_3 + f_6 + f_7)}{1 - u_x} \tag{16}$$

$$f_5 = f_7 - \frac{1}{2}(f_2 - f_4) + \frac{1}{6}\rho u_x + \frac{1}{2}\rho u_y \tag{17}$$

$$f_8 = f_6 + \frac{1}{2}(f_2 - f_4) + \frac{1}{6}\rho u_x - \frac{1}{2}\rho u_y \tag{18}$$

The Pressure (Dirichlet) boundary condition was also developed by Zou and He [26] analogously to the velocity boundaries. They calculate the unknown distribution function values using the imposed density. In this work, the conditions of this type of boundary conditions applied at the west boundary are given by the following equations:

$$u_y = -1 + \frac{1}{\rho}(f_0 + f_1 + f_3 + 2(f_2 + f_5 + f_6)) \quad (19)$$

$$f_4 = f_2 - \frac{2}{3}\rho u_y \quad (20)$$

$$f_7 = f_5 - \frac{1}{2}\rho u_x - \frac{1}{6}\rho u_y + \frac{1}{2}(f_1 - f_3) \quad (21)$$

$$f_8 = f_6 - \frac{1}{2}\rho u_x - \frac{1}{6}\rho u_y - \frac{1}{2}(f_1 - f_3) \quad (22)$$

At the east boundary condition which represents the outlet condition, the unknown distributions f_3, f_6 and f_7 are given by the following equations:

$$f_3^x = 2f_3^{x-1} - f_3^{x-2} \quad (23)$$

$$f_6^x = 2f_6^{x-1} - f_6^{x-2} \quad (24)$$

$$f_7^x = 2f_7^{x-1} - f_7^{x-2} \quad (25)$$

2.2.2. Thermal boundary conditions

Several works have been performed to implement accurate thermal boundary conditions [28-29]. Some types of boundary conditions are applied exactly in the same way as isothermal LBM models, such as open boundary conditions and periodic boundary conditions since they are intuitive.
At the west boundary, we imposed T_{in}, the unknown distribution functions g_2, g_6 and g_9, and their values are given by:

$$g_6 = T_{in}(w_6 + w_8) - g_8 \quad (26)$$

$$g_2 = T_{in}(w_2 + w_4) - g_4 \quad (27)$$

$$g_9 = T_{in}(w_9 + w_7) - g_7 \quad (28)$$

2.3. Numerical approach

The algorithm of LBM model starts with initializing the problem. The domain size is defined (number of nodes in every direction). For the case of the flow past obstacles, we should specify the diameter of the obstacle (flow past a sphere...). While for the case of porous media, we ought to specify a binary mask to distinguish the obstacles from the other part of the domain. By specifying the kinematic viscosity of the fluid and the inlet velocity, Reynolds number is calculated. After initialization, the basic steps of LBM will be computed i.e. collision and streaming. There are some boundary conditions that must be placed after the streaming step due to their role in determining the unknown distribution functions caused after streaming, and must be calculated before that particles enter in collision. Macroscopic values computation can be evaluated either after streaming or after collision. After calculating macroscopic values, a convergence test is applied to ensure the steady state. If the steady state is not reached yet, we pass to the next time step. Then, visualizations are presented. Taking into account all these conditions, the algorithm adopted is described by Figure 4.

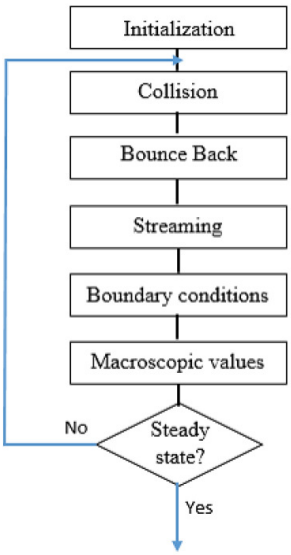

Figure 4: LBM algorithm.

Stability of LBM model is affected mainly by two important parameters which are the relaxation time τ and discrete velocity. Concerning relaxation time, there have been investigations done [30-31] to study its influence on the computation results stability. According to Eq. (2), the kinematic viscosity (ν) must be positive, otherwise the program will be instable. This condition imposes:

$$0 < \tau < 1.5 \qquad (29)$$

The discrete velocity must be kept, in practice, below or equal to 0.2 (Lattice units) to maintain the incompressibility condition of the fluid [48]. In fact, Mach number must be too inferior to unity:

$$M = \frac{U_{lb}}{c_s} \ll 1 \quad (30)$$

Where U_{lb} is the discrete velocity and c_s is the Lattice speed of sound.

At the end of the LBM algorithm, a convergence test must take place in order to be sure that the steady state is reached. The steady-state simulation is considered converged when the maximum error over the fluid nodes satisfies the condition [32]:

$$max_{\substack{i=1:N_x \\ j=1:N_y}} \frac{|U(x_i,y_j,t+1)-U(x_i,y_j,t)|}{|U(x_i,y_j,t)|} < \epsilon \qquad (31)$$

The used value of maximum error is $\epsilon = 10^{-6}$.It is well-known that it is recommended to use this type of convergence (relative) among other types such as absolute convergence except for the case when the denominator is near zero. In this work, we notice that all the simulations carried are with $|U(x_i, y_j, t)|$ not really close to zero.

For simulations carried using the real SOFC microstructure, $|U(x_i, y_j, t)|$is close to zero. Therefore, the absolute convergence is employed:

$$max_{\substack{i=1:N_x \\ j=1:N_y}} |U(x_i, y_j, t+1) - U(x_i, y_j, t)| < \epsilon \qquad (32)$$

The used value of maximum error is $\epsilon = 10^{-11}$.

3. Results and discussion

3.1. Mass diffusion LBM results

3.1.1. Flow around a sphere: Laminar viscous flow

As a preliminary step in simulating diffusion through more complex geometries, the 2D LBM model is first used to model transport of hydrogen species through a cylindrical tube parallel to the x-axis containing a sphere (Figure 5). The sphere is 10 (lu) diameter, placed in the center of the domain. Zou and He boundary conditions are applied at the inlet (velocity) and outlet (density). Periodic boundaries are applied at the top and bottom walls. Simulation parameters illustrated in Table 3.

Table 3: Simulation parameters in lattice units.

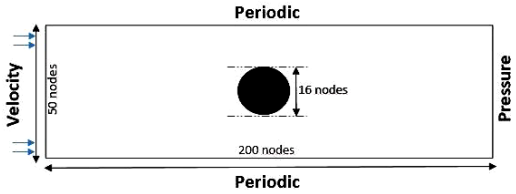

Reynolds number	0.5
Velocity ($U_{inlet,lb}$)	0.01
Viscosity (ν_{lb})	0.32
Diameter (D)	16
Density (ρ)	1

Figure 5: domain details for a flow around a sphere

In Figure 6 (a), the velocity field is presented to illustrate that LBM can easily handle the obstacles in a porous domain by the bounce-back effect for the particles at the obstacle wall. A high velocity appears at the top and bottom of the domain which are related to the confinement of the fluid between the obstacle and the wall boundary. This is in good alignment with the fact that for the same flow rate, the decrease of passage surface induces higher velocities. The lowest velocities are located around the sphere especially in the front region and the separation region. Figure 6 (b) present the streamlines around the sphere and showed that the laminar regime is proved, due to the smooth distribution of streamlines around the sphere. Flow in the wake region is not separated as there is absence of "eddies" or small packets of fluid particles.

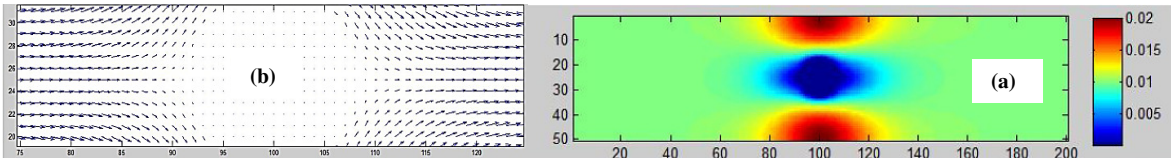

Figure 6: (a) Velocity profile and (b) streamlines around the sphere at *Re= 0.5*.

Figure 7 shows the density distribution among the domain. Density decreases slightly from inlet, where the fluid enters with its maximum density, until the outlet. This small drop could be explained by the pressure gradient driving the flow because the pressure is known to be related to density ($p = \rho {c_s}^2 = \frac{1}{3}\rho$) according to the LBM theory. Recorded density small variation results on an average density equal to unity similar to the inlet density. This confirms the incompressibility of the fluid, and proves consequently the mass conservation.

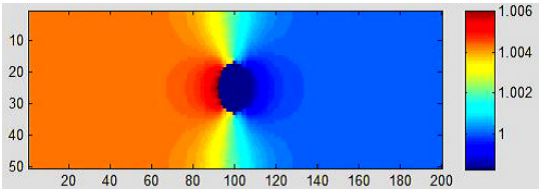

Figure 7: Hydrogen density profile in case of a flow around a sphere after 10316 iterations.

3.1.2. 2D Flow in an artificial porous media

Once the 2D flow LBM model is validated, it is used to study mass transport in the SOFC anode model. Both the spherical packing geometry and the real anode geometry are considered for analysis. The artificially build up geometry contains a randomly placed spherical obstacles representing approximately the anode material particles, between which the fuel gas will circulate. The domain is shown in Figure 8. It is 50 nodes height and 200 nodes length. The size of spherical obstacles is variable. We imposed as boundary conditions a velocity condition at the inlet, periodic boundaries on top and bottom of the domain, and a density Dirichlet boundary condition at the outlet. The domain is computed as a binary mask, the obstacles are presented by "1" and the remaining part by "0". Simulation parameters are summarized in Table 4.

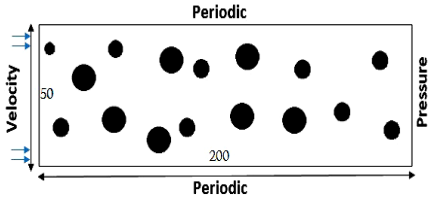

Figure 8: Domain description of the artificially anode geometry.

Table 4: Simulation parameters in lattice units.

Reynolds number	10^{-4}
Velocity ($U_{inlet,lb}$)	10^{-6}
Viscosity (ν_{lb})	0.5

Figure 9 shows that the velocities obtained at steady state are very low. Note that the velocities presented are in lattice units. The region of close obstacles is a region where velocities are almost zero due to the pressure head drop phenomena occurring at obstacle surfaces resulting of the viscous frictional forces applied by the flowing fluid on the surface of the obstacles.

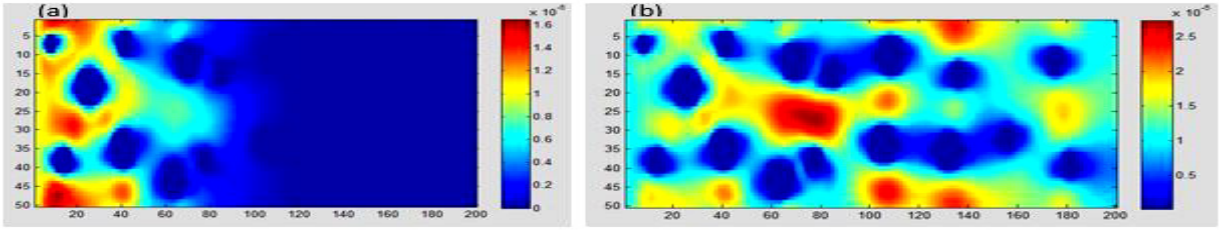

Figure 9: Velocity distribution in the porous media for (a) 155 iterations; (b) 5000 iterations.

3.1.3. 2D Flow in the real anode microstructure

In order to simulate the velocity profile through a real anode microstructure of the SOFC, SEM-scanned SOFC anode portion was used. SEM (Scanning Electron Microscopy) is a technique used to track the morphology and

chemical composition of microstructures by means of focused beam of high-energy electrons. Figure 10 shows the SEM-scanned portion of an anode SOFC cross-section realized by our research group. To enable the simulation of the real structure, dimensions have been measured using the Image J software at the given image scale. Dimensions are 20.5µm length and 14.61µm height. Furthermore, an image processing has been applied through a developed MATLAB code. This image processing consists basically of converting the image to binary then applying an operation of "opening" which is a combination of erosion and expansion steps, to finally get an approximate shape of the anode porous media structure as illustrated in Figure 10 the porosity of the treated image was estimated by Matlab script to 66%.

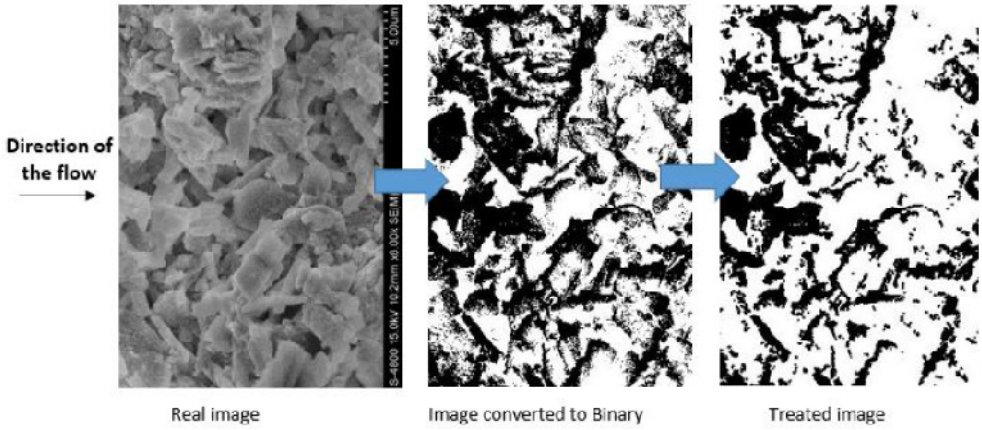

Figure 10: Anode image treatment steps. Final anode real image is on the right.

The LBM parameters used in this case are accomplished in two steps as previously mentioned; from physical system to dimensionless system, then from dimensionless system to Lattice system. Table 5 shows a summary of the physical and Lattice parameters used for the simulation of the 2D hydrogen flux through the real anode geometry of the SOFC.

Table 3: 2D LBM model parameters of hydrogen diffusion in real anode geometry.

	Physical system	Lattice system (lb)
Reynolds number : R_e	$3.14\ 10^{-4}$	$3.14\ 10^{-4}$
Velocity: U_{inlet} (m/s)	0.01	10^{-7}
Viscosity: ν (m²/s)	$0.0652\ 10^{-2}$	0.032
Length : L_x (m)	14.6	71
height: L_y (m)	20.5	100

Simulation results presenting the velocity profile through the real anode microstructure at different time steps are illustrated in Figure 11.a slow diffusion of hydrogen fuel through the porous anode domain was signaled due to the low inlet flow rate of the fuel. The fuel velocity slightly increases compared to the initial velocity ($10^{-7}lu$). This can be explained by the confinement of the fuel inside the porous structure. Tortuosity of the anode porous media is outlined. Simulation also shows that there are some parts of the domain (upper side) that are not fueled. In fact, those anodic zones seem to be characterized majorly by blocked pores rather than open ones.

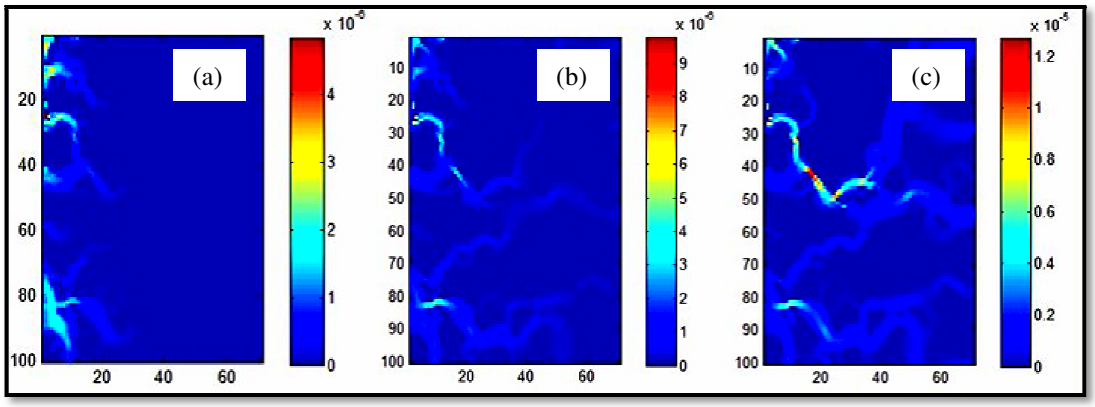

Figure 11: Velocity simulation at intermediate iteration numbers, 61, 400, 20000.

In order to evaluate the influence of porosity on the velocity profile, porosity of the real anode was modified manually using image processing. The new image obtained is given in Figure 12(b). The new anode porosity measured is about 75%.

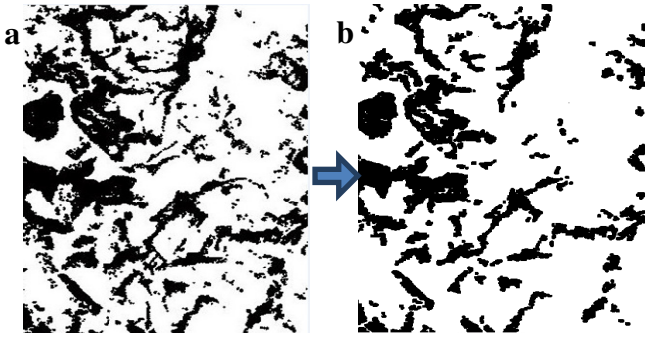

Figure 12: treated anode images (a): porosity= 66%, (b) porosity= 75%.

Figure 13 shows the velocity profile through the second real porous anode media illustrated in Figure 12(b). In comparison with Figures 11, it is clear that the higher is the anode porosity the lower is the H_2velocity. This is aligned with the increase of velocity when the fuel is bounded in narrow paths. Nevertheless, the H_2 fuel distribution seems to be more distributed when the anode porosity increases. The increase in porosity appears beneficial for the decline of the concentration polarization but it may be a source of a high activation loss as the contact between the anode particles needed for the reaction sites is quite limited in this case.

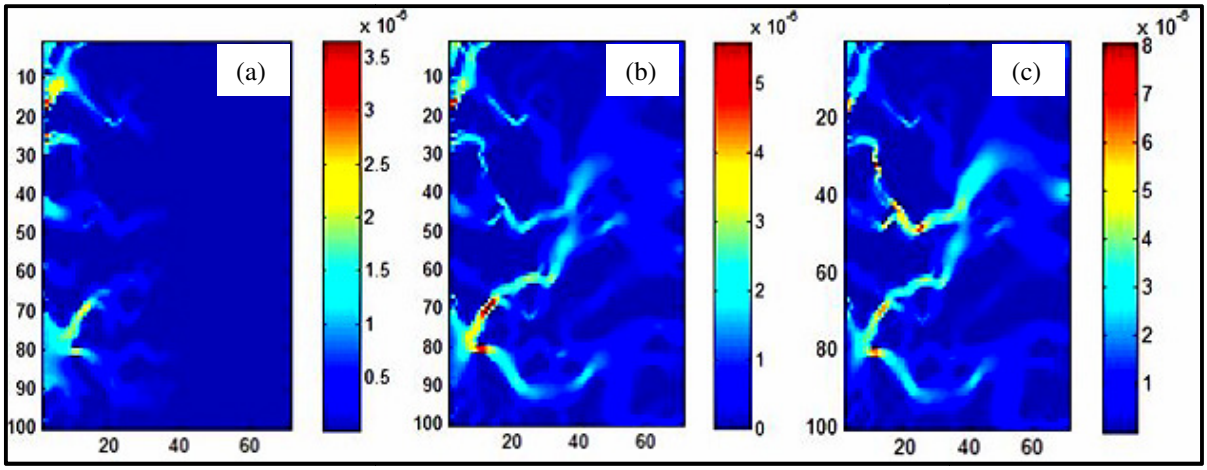

Figure 13: Velocity simulation at intermediate iteration numbers, 61, 400, 20000.

3.2. Coupled Heat and Mass transport LBM model results

3.2.1. Flow around a sphere: Laminar viscous flow

As a preliminary step in simulating temperature profile through the real anode geometry of solid oxide fuel cell, a flow around a hot sphere and hot walls was modeled. The computation domain is the same as the previous example of a flow in a channel with hot walls and cold entry, in which a hot sphere with normalized temperature equal to 1 will be added as illustrated in Figure 14. Boundary conditions for velocity and temperature fields are specified.

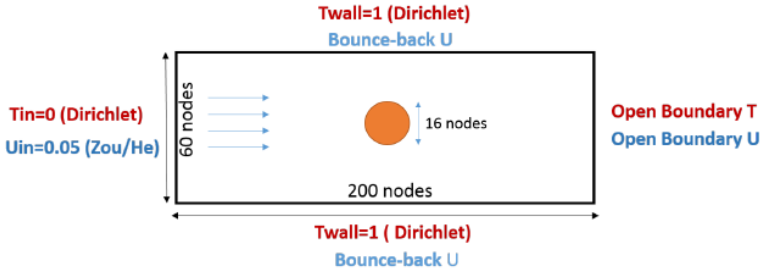

Figure 14: Computation domain description with detailed temperature and velocity boundary conditions.

Figure 15 illustrates the velocity and the temperature profiles through the rectangular channel. Results show that Hydrogen which is introduced in cold state was heated progressively by convection with heated sphere, top and bottom walls. At about x=100 (position of the sphere), the temperature is almost uniform at values between 0.9 and0.95.The increase of temperature on the surface of the sphere can be explained by the heating effect created by friction forces occurring due the contact fluid-solid. These forces convert the kinetic energy (work) into thermal energy (heat).

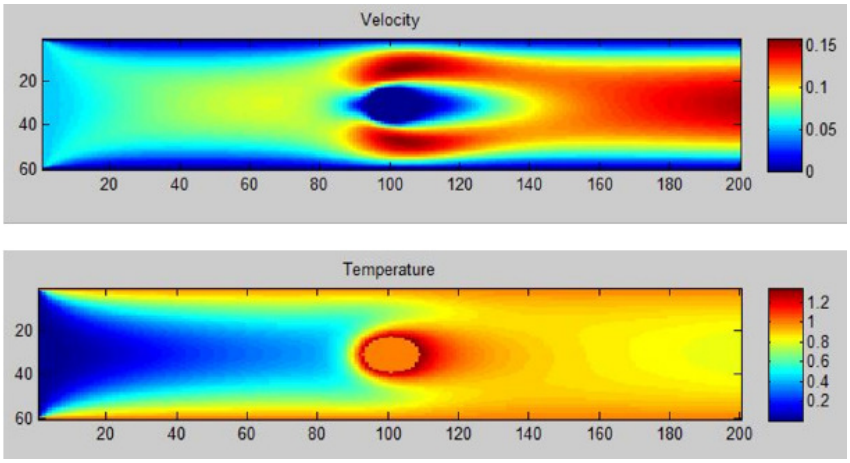

Figure 15: Velocity and temperature profiles in case of a flow around a hot sphere and hot walls.

3.2.2. Flow around a randomly placed hot spheres

In a continuous approach to get closer the SOFC anode porous structure, another example was simulated. A flow past an artificially generated porous media was modeled. A velocity boundary condition is imposed at the inlet. At the outlet, open boundary is applied. Top and bottom boundaries are set as periodic for velocity field. The thermal boundary conditions of top and bottom walls are adiabatic. Flow at the inlet is cold and set to 0 normalized temperatures by means of a Dirichlet boundary condition. The outlet is an open boundary. Spheres or obstacles are at high temperature (normalized temperature=1).

Simulation results are illustrated in Figure 16. It is noticed that the more the fluid progresses inside the channel the more it is heated. In fact, the contact with the first spheres at x=50 and x=75 rises the temperature from 0 to 0.7. At the contact of fluid with the later obstacles, temperature 1 is reached. The hydrogen particles' surrounding the hot obstacles is blocked (velocity nill) and exhibits a temperature higher slightly than the normalized obstacle temperature.

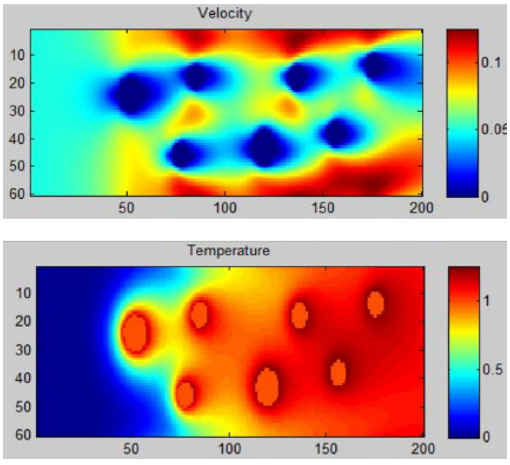

Figure 16: Velocity and temperature profiles in case of an artificially porous media.

3.2.3. Flow in the real anode porous geometry

Simulation of velocity and temperature profiles was applied to the real anode structure presented in Figure 12(a). Simulation parameters are those given in Table 3. The porous domain of the fuel cell is initially heated to 600°C. In fact, before feeding the device with fuel, it is necessary that the fuel cell reaches a high temperature since it is an essential operating condition for the activation of anodic electrochemical reactions. The porous structure is at a normalized temperature set to unity, the inlet fuel is cold and set to 0. Top and bottom boundaries are adiabatic.

Open boundary condition is applied at the outlet of the domain. Simulation results illustrating H_2 velocity profile and temperature distribution are shown in Figure 17. The temperature distribution among the domain is almost uniform except for the inlet where the cold fluid hardly diffuses, as illustrated in velocity profile too. According to the literature, a series of exothermic reactions could take place in the anode which may results in a temperature distribution slightly different especially near electrochemically active areas.

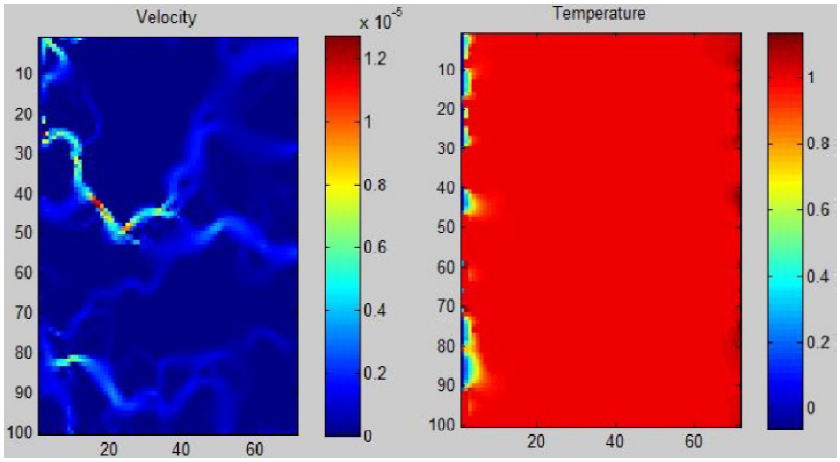

Figure 17: Hydrogen velocity and temperature profiles inside the real anode geometry.

Conclusion

A 2D LBM model was developed to model mass transfer through porous materials. Based on the SEM micrographs, it is now possible to reconstruct the pore structure of a SOFC anode with a clear identification of solid and pore phases. The treated image data were used as input to the LBM model to simulate temperature profile and mass transport of hydrogen fuel through the pores along the anode thickness.
Mass transport results, generated using the real anode porous geometry, agree with results from simpler geometries generated using a unique sphere and a randomly spherical packing model. The 2D coupled heat and mass transport LBM model developed in this work may be part of a series transport models that can eventually be used for geometry optimization of the SOFC electrodes. According to the obtained results, it appears that in order to accurately predict the mass and thermal transport phenomena taking place inside the porous anode media, it is recommended to take into account a detailed description of electrochemical aspects existing inside the anode microstructure. Therefore, a coupled electrochemical model to the already build mass and thermal lattice Boltzmann method, will be one of the major perspectives of this work.

Nomenclature

List of symbols

D Particle diameter, m
L_x Length of the domain, m
L_y Height of the domain, m
K_B Boltzmann constant, $m^2.kg.s^{-2}.K^{-1}$
m Weight, Kg
Re Reynolds number, -
t Time, s
x, y Position, m
f Particle distribution function, mass transport
g Particle distribution function, heat transport
ρ Density, $Kg.m^{-3}$
T Temperature, K
u_x Velocity in x-direction, $m.s^{-1}$
u_y Velocity in y-direction, $m.s^{-1}$
u Velocity vector, $m.s^{-1}$
c Celerity, $m.s^{-1}$
ℓ Domain length in lattice unit, -
c_s Celerity of sound, $m.s^{-1}$

Greek symbols
α Thermal diffusivity, $m^2.s^{-1}$
ν Kinematic viscosity, $m^2.s^{-1}$
τ Relaxation time, -
ω Weight factor, -

Indices
d Dimensionless system
lb Lattice unit system

References:

[1] W.K.S. Chiu, A.S. Joshi, and K.N. Grew, Lattice Boltzmann model for multi-component mass transfer in a solid oxide fuel cell anode with heterogeneous internal reformation and electrochemistry, *Eur. Phys. J. Special Topics,* Volume 171, Pages 159–165, 2009.

[2] A. Lanzini , P. Leone, P. Asinari , Microstructural characterization of solid oxide fuel cell electrodes by image analysis technique, *Journal of Power Sources*, Volume 194, Pages 408–422, 2009.

[3] A.S. Joshi, K.N. Grew, J.R. Jr. Izzo, A.A. Peracchio, W.K.S. Chiu, Lattice Boltzmann Modeling of Three-Dimensional, Multicomponent Mass Diffusion in a Solid Oxide Fuel Cell Anode, *ASME J. Fuel Cell Sci. Tech.,*Volume 7, Pages 1-8, 2010.

[4] K.N. Grew, A.S. Joshi, A.A. Peracchio, W.K.S. Chiu, Pore-Scale Investigation of Mass Transport and Electrochemistry in a Solid Oxide Fuel Cell Anode, Journal of Power Sources, Volume 195, Pages 2331-2345, 2010.

[5] A.S. Joshi, A.A. Peracchio, K.N. Grew,W.K.S. Chiu, Lattice Boltzmann Method for Multi-Component, Non-Continuum Mass Diffusion, *J. Phys. D: Appl. Phys.*, Volume 40, Pages 7593-7600, 2007.

[6] A.S. Joshi, K.N. Grew, A.A. Peracchio, W.K.S. Chiu, Lattice Boltzmann Modeling of a 2D Gas Transport in a Solid Oxide Fuel Cell Anode, *Journal of Power Sources*, Volume 164, Pages 631-638, 2007.

[7] A.S. Joshi, A.A. Peracchio, K.N. Grew, W.K.S. Chiu, Lattice Boltzmann Method for Multi-Component Mass Diffusion in Complex 2D Geometries, *J. Phys. D: Appl. Phys.,* Volume 40, Pages 2961-2971, 2007.

[8] K.N. Grew, A.S. Joshi, W.K.S. Chiu, Direct Internal Reformation and Mass Transport in the Solid Oxide Fuel Cell Anode: A Pore-scale Lattice Boltzmann Study with Detailed Reaction Kinetics, *Fuel cells*, Volume 10, No. 6, Pages 1143–1156, 2010.

[9] Y. Guan, X. Song, G. Liu, Z. Liang, L. Chen, X. Zhang, Y. Xiong, S. Chen, Y. Gong, H. Wang , Y. Tian, Lattice-Boltzmann modeling of gas transport in Ni-Yttria-stabilized zirconia anodes during thermal cycling based on X-ray computed tomography, *Electrochimica Acta*, Volume 121, Pages 386–393, 2014.

[10] A. L. Garcia, G. R. McNamara, B. J. Alder. Stabilization of thermal latticeboltzmann models. *J. Stat. Phys.*, Volume 81, Pages 395, 1995.

[11] M.A. Abbassi, A. Omri, I. Mejri, A. Mahmoudi, Radiation heat transfer effect in solid oxide fuel cell: Application of the Lattice Boltzmann method, *International Journal of Mathematical, Computational, Physical, Electrical and Computer Engineering*, Volume 8, No.4, Pages 632-636, 2014.

[12] I. Mejri, A. Mahmoudi, M.A. Abbassi, A. Omri, LBM simulation of Heat transfer in Solid Oxide Fuel Cell, *International Journal of Heat and Technology*, Volume 34, Pages 351-356, 2016.

[13] X. Shan, Simulation of rayleigh-bénard convection using a lattice Boltzmann method, *Physical Review E* Volume 55, No. 3, Pages 2780-2788, 1996.

[14] P. Lallemand, L.S. Luo, Hybrid finite-difference thermal Lattice Boltzmann equation, International Journal of Modern Physics B, Volume 17, Pages 41-47, 2003.

[15] X. He, S. Chen, G.D. Doolen, A novel thermal model for the lattice Boltzmann method in incompressible limit, *Journal of Computational Physics*, Volume 146, Issue 1, Pages 282-300, 1998.

[16] Y. Peng, C. Shu, Y. T. Chew, Simplified thermal lattice Boltzmann model for incompressible thermal flows. *Physical Review E*, Volume 68, Pages 026701, 2003.

[17] A. D'Orazio, S. Succi, Simulating two-dimensional thermal channel flows by means of a lattice Boltzmann method with new boundary conditions, *Future Generation Computer Systems*, Volume 20, Pages 935-944, 2004.

[18] Y. Shi, T.S. Zhao, Z.L. Guo, Thermal Lattice Bhatnagar-Gross-Krook model for flows with viscous heat dissipation in the incompressible limit*, Physical Review E*, Volume 70, Pages 066310, 2004.

[19] C. S. Nor Azwadi, T. Tanahashi, Simplified thermal Lattice Boltzmann in uncompressible limit, *International Journal of Modern Physics B*, Volume 20, No. 17, Pages 2437–2449,2006.

[20] J. V. Neumann, The general and logical theory of automata, Collected works. Pergamon Press, Volume V, 1963.
[21] J. V. Neumann, Theory of self-reproducing automata. University of Illinois Press, 1966.
[22] M. Groppi, G. Spiga, A Bhatnagar Gross Krook-type approach for chemically reacting gas mixtures, *American Institute of Physics*, Volume 16, No. 12, Pages 4273-4284, 2004.
[23] D. d'Humieres, Generalized Lattice Boltzmann equations. Rarefied gas dynamics: theory and simulations, *Progress in Aeronautics and Astronautics*, Volume 159, Pages 450-458, 1992.
[24] J. Latt, Hydrodynamic limit of lattice Boltzmann equations, PhD thesis, Univ. Genève, 2007.
[25] A.A. Mohamad, Lattice Boltzmann Method: Fundamentals and Engineering Applications with Computer Codes, ISBN 978-0-85729-455-5, 2011.
[26] Q. Zou, X. He, On pressure and velocity boundary conditions for the Lattice Boltzmann BGK model, *Phys. Fluids*, Volume 9, No. 6, Pages 1591-1598, 1997.
[27] J. Latt, Choice of units in Lattice Boltzmann simulations, *http://wiki.palabos.org/_media/howtos:lbunits.pdf, April 2008.*
[28] C.H. Liu, K. H. Lin, H.C. Mai, C.A. Lin, Thermal boundary conditions for thermal lattice Boltzmann simulations, *Computers & Mathematics with Applications*, Volume 59 , Pages 2178–2193, 2010.
[29] L. Li, R. Mei, J.F. Klausner, Boundary conditions for thermal Lattice Boltzmann equation method, *Journal of Computational Physics*, Volume 237, Pages 366-395,2013.
[30] M. Schreiber, GPU based simulation and visualization of fluids with free surfaces, PhD thesis, Univ. Munchen, 2010.
[31] J.D. Sterling, Stability analysis of lattice Boltzmann methods, http://arxiv.org/pdf/comp-gas/9306001.pdf, 1993.
[32] C. Ronald, R. Scherer Bogdan Kucinschia, Abdollah A. Afjeh. On the application of the lattice Boltzmann method to the investigation of glottal flow, *Journal of Acoustical Society of America*, Volume 124 (1), Pages 523-534, 2008.